State of art for LASer Adhesion Test (LASAT)

L. BERTHE[1*], M. ARRIGONI[2], M.BOUSTIE[3], J.P CUQ-LELANDAIS[3], C. BROUSSILLOU[4], G. FABRE[4], M. JEANDIN[4], V. GUIPONT[4] M. NIVARD[1]

1. Laboratoire Procédés et Ingénierie en Matériaux et Procédés, UMR CNRS/ARTS ET METIERS 8006, 151 Boulevard de l'Hôpital, 75013 Paris Cedex
2. Laboratoire Brestois de Mécanique et des Systèmes LBMS (EA 4325, ENSIETA / Université de Brest / ENIB) ENSIETA – MSN 2 Rue François Verny, 29806 Brest Cedex 9 FRANCE
3. PPRIME-ENSMA – Université de Poitiers - UPR CNRS 3346 – 1 Av. Clément Ader, Téléport 3, 86961 Futuroscope Cedex, France
4.MINES ParisTech, Centre des Matériaux, CNRS UMR 7633, Centre de Compétence en Procédés de Projection, BP 87, 91003 Evry Cedex, France

* Corresponding author, lberthe@gmail.com, Tél. : +33 1 71 93 65 38

State of art for LASer Adhesion Test (LASAT)

Keywords: laser, shock, adhesion test,

This paper proposes a state-of-art on laser adhesion test. It consists in testing material interfaces with laser driven shock wave. Since first demonstration in 80’ by Vossen, many studies and development have been done. This paper presents recent experiments and developments on basic physics involved. Results show the ability of the technique to do a quantitative adhesion test for wide range of material and configuration. Edge effect principle and ultra-short shock wave give perspectives for new applications for multi-layer combination of material. Fundamental principles are evidenced through experiments on bulk ductile materials before demonstrating their application to coated systems.

1. Introduction

The LASer Adhesion Test (LASAT) concerns the adhesion test of coatings. It is a no contact technique to generate high-level and tensile stress at an interface. Figure 1 shows a schematic view of LASAT. The technique uses a shock wave produced by plasma induced by laser pulse, inside a couple substrate/coatings to be tested. The reflection of this waves at the rear free surface yields to tensile stresses inside the target. If it is high enough, this traction can produce the debonding of the interface.
The failure diagnosis can be realized using the measurement of the Rear Free Surface Velocity (RFSV) (by a Velocimeter Interferometer for Any Reflector for example)[1,2,3] , or by direct visualisation of the coating[4,5], or Ultrasonic techniques[6].
For a given coated system and a laser duration, a laser intensity limit is determined by increasing the laser power density (in $GW.cm^{-2}$) up to the first one for which debonding occurs. The adhesion strength is also quantified with numerical simulation of shock wave propagation inside the material reproducing experimental data. It could be used as a nondestructive test when interfaces are sollicitated with stresses below the adhesion threshold.

LASAT is an application of the laser spallation process that was introduced in the 80's by Vossen[7] to spall coatings by shock wave. Yuan and Gupta[8] proposed the first quantitative approach in the case of thin film and using sub-nanosecond laser pulse. More recently refs 9, 10, 11,12,3 and 4 validated models for the quantitative interface strength measurement for thermal spray coatings. In 2007, Boustie and al[13] introduced edges effects around the laser impact. It opens perspectives for the test of real parts including generally thick substrates.
This paper proposes a short review on last advances on LASAT. The second part reviews the experimental configuration of shock wave production by laser. The third part concerns a state of the art on basic LASAT. Part 5 and Part 6 present new configurations of the adhesion test for thin and thick coating using ultra-short laser and edge effects respectively. In both cases, the fundamental principles involved are first evidenced through experiments on bulk ductile materials before demonstrating their application to coated systems.

2. Laser driven Shock wave

The laser driven shock waves principle is well known in a range of moderate intensity[14,15]. Short and intense laser impact ((typical ranges 1 – 40 joules for energy, 3 to 20 ns for duration and 1-300 $GW.cm^{-2}$ for power density) induces the target ablation surface into a high pressure plasma (GPa). Its fast expansion generates a compressive wave inside the target by the action / reaction principle.
Two set-ups can be used: direct or confined irradiation such as described in Figure 1 and Figure 2 respectively. In the direct regime, interaction is performed in vaccum. In the confined regime, the expansion of the plasma is limited by the presence of the confining matter (typically water or glass). This configuration allows to generate pressure about four times higher and two times longer than in direct regime for the same laser parameters (Peak power density, pulse duration, wavelength). However, the drawback of this technique is the screening of the target by the breakdown in the confining medium occurring at high power density.
For LASAT, the confined regime has a very good potential because it requires lower energy than direct irradiation and therefore rather compact laser system can be used.

The link between laser and stresses loading profiles in the target is computed by Laser / matter interaction codes in direct regime (for example FILM (based on SUPER and MEDUSA codes[16]) and in confinement regime[17]. More recently, specific development have been experimentally validated for ultra short laser by Cuq-le Landais[18.]

3. Basics for LASAT

3.1. Basic description

The classical mechanism leading to dynamic fracture inside a material with shock wave is reminded in the space vs. time and pressure vs. particle velocity diagrams of the Figure 3a and b respectively. Numbers on space vs. time correspond to number of state on pressure vs. particular velocity diagram.
For a first approach of the phenomena, a simple shock wave analysis with acoustic approximation is performed like fully described in ref 19. Laser impact generates a compression wave (A - from state 0 to state 1) which is followed by a release wave (B - from state 1 to state 2). These two waves propagate through the target. First, wave (A) reaches the rear free surface and is reflected in another rarefaction wave (C- from state 1 to state 3). When the two rarefaction waves (C) and (B) intersect, the tensile stress level state 4 is produced. This one can damage the target on weak points or at the initiation point of this state (release waves crossing F1). This dynamic fracture is also called “spallation process”.
For a target including substrate+coating, similar mechanisms can lead to dynamic fracture at the interface. Indeed, this one occurs according to the level of tensile state and the adhesion of the coating.

3.2. Numerical tools

These basic phenomenas could be simulated by numerical code for many years in homogeneous material. HUGO, developped by Bolis and al[3], is based on the simplest formulation with acoustic propagation in hydrodynamic medium[19]. With this acoustic approximation, shock waves and releases propagate at the sound velocity and therefore no decay of shock can occur. From HUGO, space vs. time, pressure vs. particule velocity diagrams and RFSV can be extracted and compared to experimental data.
SHYLAC[20] is a 1D finite difference code solving hydrodynamics conservative laws inlcuding a Mie-Grüneisen equation of state, a perfectly elasto-plastic constitutive law for metallic materials and damage and failure criteria. SHYLAC gives the state of matter at any time and any location in the target. Particularly, stress loadings at the interface between coating and substrate can be extracted from the code.
Commercial codes as RADIOSS or Abaqus®/explicit extend to multi-dimensionnal analysis of shock wave propagation, allowing the description of edge effect and complex materials.
For applications, HUGO gives a better understanding of waves propagation and a qualitative modelisation allowing elementary velocity profile analysis like in part 3.3. SHYLAC and RADIOSS give a realistic quantitative tensile stress adhesion threshold in agreement with experimental profiles.

3.3. Experimental validation

Figure 4 and Figure 5 (From ref. 3) present a schematic space vs time diagram (see part 3.1) and RFSV measurements for Cu substrate and electrochemical coating Ni

couple at power densities 79 GW.cm^{-2} and 370 GW.cm^{-2} respectively. HUGO calculations and SHYLAC simulations (see part 3.2) are also presented.
On (space-time) diagram, state numbers close to the free surface correspond to peak numbers on the velocity profile. F1 is the intersection between the two rarefactions waves which can induce the fracture phenomena and F2 is the intersection of the tensile stresses wave generated at the interface
On Figure 4 b, experimental measurement and corresponding numerical simulation by SHYLAC show two positive peaks at 70m.s^{-1} : the first emergence (peak 1) of the incident and its second emergence (peak 4) after following the crossing of the entire target as on (space-time) diagram and HUGO calculation. The time difference between Peak 1 and peak 4 corresponds to two transit times of shock wave in the whole target ($2x(C_o^{Cu}.th_{Cu}+C_o^{Ni}.th_{Ni})$=103ns), where C_o^{Cu} (=3933 m/s) is the bulk sound velocity of Cu, th_{Cu}(=119 um) is thickness of Cu substrate, C_o^{Ni} (=4919 m/s)is the bulk sound velocity of Ni, th_{Ni} (=88 um) is the thickness of Ni coating. These peaks diagnose the absence of interface fracture before this time.
Peak 2 corresponds to the main wave reflections on the interface between Cu and Ni. Its comes from the reflection at the interface of the wave from the rear surface and Ni/Cu interface. The peak 2 is a rarefaction wave inducing a negative peak velocity.
The agreement is rather good between SHYLAC simulation and the experimental profile. Simulation reproduces the main emergences: first and second positive peaks (1 and 4) and negative peak at 124 ns.
Only on HUGO simulation, a small positive peak (numbered 3) appears at 106ns (10m/s). It is produced by the return from the front face of the first wave reflection at the interface. These differences for peaks emergence come from acoustic approximation and schematic pressure profile used in HUGO calculations or edge effects around the laser impact (Part 5).
On Figure 5, at higher laser intensity leading to the Ni coating debonding, a rather good agreement between experimental RFSV and the corresponding numerical simulation SHYLAC and HUGO approach is observed. Positive peaks 1, 2’ and 2” provided by HUGO approach are reproduced.Peak 1 is the first emergence of the incident shock wave.Peak 2’ and 2”are the incident release coming from the rear surface and the reflection at the fracture as a compressive wave.They are the signature of the coating debonding. The debonding strength (σ_d) can be evaluated from Ref. 19 :

$$\sigma_d=\frac{1}{2}\rho_0 C_0 \Delta u \qquad \text{Equation 1}$$

Where ρ_0 is the density of material, C_o is the bulk sound velocity and Δu is Δu is the velocity jump from the top of the peak to the take off point.
Using Cu or Ni properties respectively σ_d is 1.28 GPa and 1.23 GPa respectively in agreement with simulations. So, experimental RFSV reproduced by physical simulation gives clearly the signature of the debonding coating and a quantitative evaluation of the debonding strength.

4. Ultra-short laser for thin coating.

4.1 description

The thickness of the spall produced by shocks e_s is directly related to the sample initial thickness L, the shock duration τ, the sound velocity c and material velocity u_1 [21]:

$$e_S = \frac{c+u_1}{2c}\left[c\tau + \left(1-\frac{c+u_1}{2c}\right)L\right] \qquad \text{Equation 2}$$

Therefore, depending on the shock generator used and the subsequent parameters (mostly shock duration and amplitude related to material velocity), different ranges of spall thickness and velocity can be covered.

With a gas gun accelerated plate generating a shock with duration in the microsecond range, spall thickness will be in the mm to cm range.

In order to test coatings within the range <50µm laser shocks appear as the most convenient shock generator. They offer possibilities of driving very high pressure shocks (up to the Mbar range) with a wide span of short durations (from femto-seconde to few nanoseconds). Therefore, their ability to test adhesion in the <50µm microns range with high velocities of hundredths of m/s has already been widely demonstrated in ns pulse duration (Part 3)

For ultra-short irradiation, Tamura et al. obtained spallation in fine aluminum targets with some fs laser pulse [22]. More recently, rear free surface velocity measurements has been reproduced by simulations including a two temperatures model (2TM) [23] describing the electron-ion non-equilibrium state for ultra-short laser matter interaction by Cuq-Lelandais[18]. Figure 6 shows a SEM picture of a rear surface of 50 µm thick aluminum target (pulse duration: 300fs, power denstiy: 0.56PW/cm ²).The measured average thickness is 10.5 ± 0.5 µm. It is in agreement with simulation reproducing RFSV presented in Figure 7 for the same target. This figure compares simulation including or not 2TM and damage model. It shows clearly the validity of models in reproducing the first peak of velocity and the constant velocity of spall flight. The spall threshold can be estimated on the free surface velocity using Equation 1. It gives 36 GPa for aluminium foil of 50 um in agreement with litterature[24].

4.2 Demonstrative applications: test of thin coatings.

In 2010[25], test adherence of thin coatings has been also performed using ultra-short irradiation. Samples tested are multi-layer systems including a molybdenum metallic layer and a chalcopyrite $CuInSe_2$ semi-conductor film deposit on soda-lim glass substrate. This film is considered as one of the most promising for thin film solar cells with record efficiencies as high as 19,9%. Direct observations of sample and RFSV measurements using shadowgraphy diagnostic has been analysed with 1D simulation using SHYLAC code. The debonding threshold is a parameter of simulations to reproduce the experimental flight velocity. Figure 8 shows space time diagram corresponding to experiment with power density above debonding threshold. RFSV and threshold is reported on diagram. This experiment/calculation approach gives different threshold for the two layers, 550 MPa and 180 MPa for soda-lim glass Molybdenum and Molybdenum chalcopyrite $CuInSe_2$ interfaces respectively.

These results show the actual ability of LASAT to produce a quantitative test using specific diagnostics and a basic knowledge on laser shock wave propagation in solid materials.

5.Edge effects

5.1.Description

When applying a shock produced by laser, a main shock wave is induced in the axial direction (laser axis) (see Figure 9-a (from ref.13)and also radially out of the laser(see Figure 9-b spot. Along the laser spot, radial compressive waves propagate towards a free surface with no pressure condition. Therefore, this radial shock wave is released by a rarefaction wave) (see Figure 9-c). maintaining the null pressure of the free surface out of the laser spot. This release propagates spherically from the edge of the spot After a propagation duration related to the spot size and the material properties, these release waves overlap around the axis of the target, producing an increased tensile stress at this location (see Figure 9-d).

Besides, a release wave is applied on the sollicitated spot, just behind the main shock. It is crossed by the previous radial release wave leading to a traction wave which propagates towards the center of the target and altering by the same time the compression front.

Depending on the resistance of the material, it could be damaged by this tensile concentration. This phenomenon could be essential for future applications of LASAT test. Indeed, the interface is sollicitated by a tensile stress produced without reflection of incident shock wave at a free surface as shown in part 3.1. The location of traction depends on the laser spot diameter, the maximum applied pressure and the material's mechanical properties. Another application is presented in part 5.3. for Thermal Barrier Coatings systems.

5.2 Experimental evidence of Edge effects

In order to evidence the impact of edges effects on shock waves propagation[13], experiments have been carried out on aluminum targets 2mm thick with an quasi-identical laser power density of 2TW/cm^2, but one shot with a focused laser spot of 1mm (2D configuration) and the other of 4mm (1D configuration). So, the only difference will be induced by the ratio spot diameter/sample thickness: 2 and ½ respectively. For the 1D configuration (Figure 10-a), we observe a classical spall completely ejected on the back free surface[14],. For the 2D configuration (Figure 10-b) with the same initial shock loading, no spall is visible on the cross section near the back of the target. Meanwhile, a damaged zone with small voids appears near the loading side.

Figure 11 presents the rear surface velocity history in 2D configuration and a comparison with Radioss simulations performed with and without damage criterion (Tuler Butcher, Ref 19). The calculated damage is much stronger than the observed one inside the sample (Figure 10-b). By simulation, the amplitude of the negative velocity is therefore much released by this fracture compared to the simulated case with no fracture. Therefore, this evidences the strong coupling of the damaging induced by these 2D effects and the measured or simulated velocity signal. The Radioss simulation with Tuler-Butcher criterion produces a full fracture around the loaded zone and not at all near the back face. This is consistent with cross-section observation for locating the damage zone, but not accurate enough for reproducing the exact pattern of voids opening and growth near the threshold observed.

5.3 Demonstrative application

In 2009, adhesion test using laser shock has been performed on Thermal Barrier Coatings systems (TBCs). It is Ni based superalloy (AM1) plates with (Ni,Pt)Al bond coat substrates and ceramic coating (7YSZ) of 150 µm thickness . Shock is generated in laser confined interaction regime on the substrate. The Figure 12a exhibits the rear surface of the target tested. The failure occurred at 7YSZ/alumina interface, or at the alumina/bond coat interface or also could be located through the alumina layer. When laser intensity increases (above the LASAT threshold), the shock wave induced one interfacial crack, but the coating remained attached to the rest of the ceramic, leading to a humped region. In this particular case, a change in whiteness of the 7YSZ is observed like in the Figure 12a . For very high laser intensities, coating ejection has been observed (a ceramic chip is created and removed from the substrate). The whitened spot size increases with increasing laser intensity as shown in Figure 12b. At 1 GW/cm^2 the whitened spot diameter is 1 mm and 4 mm at 2.5 GW/cm^2. This protocol has been also demonstrated for Hydroxyhapatite coating in ref 4.
The size of white spot is related to the edge effects previously discussed. The extension of axial shock wave is due to propagation of lateral wave from the edge (see Figure 13a). By reflection on the free surface (YSZ/air), Figure 13.b, 1D wave propagates in the opposite direction, crossing through the alumina of 3µm thick.. In Figure 13.b, edge effects on the stress distribution along the radial axis after the shock wave reflection are described by the color map. The Figure 13.c exhibits the stress distribution at the interface from shock axis in the radial direction. The planar 1D wave induces a constant stress level only near the shock axis whereas a stress decreasing due to lateral edge effects is observed. From this LASAT FE model, reducing failure criteria value will increase the damaged interface radius for a given stress level and increasing the initial applied stress will increase the crack size.

6.Conclusions.

This paper reviews a state-of-art on laser adhesion test. Recent experiments and developpement show clearly the ability of shock wave induced by laser to test coatings in wide range of materials. Progresses on basic phenomenas, numerical simulations and diagnostics allow, now, a quantitative adhesion test (part 3.4). However, new configurations (like edge effects) and new range of parameters provided by laser technologies give perspectives for new applications. In playing with spatial and temporal of laser loadings, it is possible to test coatings on thick substrate (part 5.2) or multi-coatings (part 4.2.). Besides, these new advances improve protocol. For example, according to material properties, one shot gives the debonding threshold of coating (part 5.3). These researches demonstrated the promising future for LASAT for the test of multi-layers and multi-material combination.

Acknowledgements

Laser experiments were performed on LULI (CNRS/Ecole polytechnique – France) ALISE (CEA –Le Barp) facilities through french national Institut Laser Plasma.
French Project LASAT was supported by CEA, CNRS and Mat&Pro Network.

References

1 Zhou M, Zhang YK, Cai L, Shen ZH and Zhang SY, 2003, *Surface coating and technology*, **165(2)** pp 146-153

2 Gupta V, 1995 System and method for measuring the interface tensile strength of planar interfaces, US patent, 5,438,402,

3 Bolis C, Berthe L, Boustie et al 2007, *J Phys D: Appl Phys* 40:3155-3163.

4 Guipont V, Jeandin M et Al, 2010, accepted in Journal of Biomedical Materials Research (2010)

5 Fabre G, Guipont V., Jeandin M., Boustie M., Cuq-Lelandais J.P, Berthe L., Pasquet A., Guedou J-Y., European Symposium on Superalloys and their Applications, 25-28 May 2010. Educational Center Wildbad Kreuth, Germany

6 Arrigoni M, Monchalin JP, Blouin A, Kurger SE, Lord M, Measur. Sci., Tech, 20(1), 015302

7 Vossen JL, 1978 *ASTM Spec. Techn. Publ. Amer. Soc. for testing and mat.*, **640** 122-133

8Yuan J and Gupta V. 1993 *J. Appl. Phys*. **74(4)** 2388-2396, Gupta V. and Yuan J. 1993 *J. Appl. Phys*. **74(4)** 2397-24104, Yuan J and Gupta V. 1993 *J. Appl. Phys*. **74(4)** 2405-2410

9 Boustie M, Auroux E, Romain JP, Bertoli A, Manesse D. Determination of the bond strength of some microns coatings using the laser shock technique. EPJ Appl Phys 1999;5:149-153.

10 Wang J, Weaver RL, Sottos NR. ,2002, Exp Mech;42:74-83.

11 Barradas S, Jeandin M, Arrigoni M, Boustie M, He H L, Bolis C and Berthe L 2004 *J. of Mat. Sci.* **39** 2707-2716

12 Barradas S, Molins R, Jeandin M, Arrigoni M, Boustie M., Bolis C, Berthe L and Ducos M 2005 *Surface and Coatings Technology* **197** 18– 27

13 M. Boustie, J.P. Cuq-Lelandais, L. Berthe, C. Bolis, S. Barradas, M. Arrigoni, T. de Resseguier , M. Jeandin 2007, J. Phys. D: Appl. Phys. 40No 22 7103-7108

14 Tollier L, Fabbro R and Bartnicki E 1998 *J. Appl. Phys.* **83(3)** 1224-1230

15 Berthe L, Fabbro R, Peyre P, Tollier L. and Bartnicki E, *J. Appl. Phys.* **82(6)** 2826-2832

16 Christiansen JP, Ashby D E T F and Roberts K V, 1974 *Computer physics comm.* **7** 271-287

17 Sollier A, Berthe L and Fabbro R, 2001 *Eur. Phys. J. Appl. Phys.* **16** 131-139

18 J.P. Cuq-Lelandais, M. Boustie, , L. Berthe, T. de Rességuier, P Combis, M. Nivard, A. Claverie 2009, J. Phys. D: Appl. Phys. 42 No 065402

19 Antoun T, Seaman L, Curan D R, Kanel G I, Razorenov S V and Utkin A V 2003 *spall fracture* (Springer-Verlag, New York) pp 49-55

20 Cottet F and Boustie M, 1989, J. Appl. Phys. 66(9) 4067-4073

21 M. Boustie, L. Berthe, S. Barradas, T. de Resseguier, P. Combis, M. Jeandin, M. Nivard, A. Claverie, SMT11…

22 Tamura H, Kohama T, Kondo K and Yoshida M, 1998 *J. Appl. Phys.* **83** 1224

23 Colombier J P, Combis P, Stoian R and Audouard E, 2007 *Phys. Rev. B* **75** 104105

24 Moshe E et al, 1998 *J. Appl. Phys.* **83** 4004

25 J.P. Cuq-Lelandais, C. Broussillou, L. Berthe and al 21st ABM-TMS International Materials Congress – Dynamic Behaviour of Materials, 26 to 30 July 2010, Rio de Janeiro - Brazil

Figures caption :

Figure 1 : General principle of LASAT technique in direct regime

Figure 2 : Shock wave production by laser plasma in confined regime

Figure 3 : (a) Schematic Space vs. time diagram for a single material target (shock wave in plain line, release wave in dashed line) (b) corresponding stress vs. particle velocity diagram (Hugoniot). Letters correspond to front waves and numbers to pressure states from pressure vs. particle velocity diagram (see text). A : front shock wave - from state 0 to state 1), B : Release wave - from state 1 to state 2, C: reflection of A at the rear free surface - from state 1 to state 3. D: reflection of B on the rear free surface - from state 4 to state 0. F1 : release waves B and C cross each other (state 4). (From ref 3)

Figure 4 : (a) Schematic (square pressure loading) space vs. time diagram (shock wave in plain line, release wave in dashed line, black color : high pressure or tensile stress, gray color : low pressure or tensile stress) and (b) experimental and caculated by HUGO and SHYLAC free surface velocity, without coating debonding. 1 : pull-back due to incident shock wave. 2 : pull back due to the reflection at the interface of the incident wave from the rear surface and peak. 3 pull back due to the return from the front face of the first wave reflection at the interface. 4 : pull back the incidence shock wave after crossing the whole target (one back and one forth). Substrate : Cu, coating : Elecrochemical Ni (125 um), Power density is 79 GW/cm^2. (From ref 3)

Figure 5 : (a) Schematic (square pressure loading) space vs. time diagram (shock wave in plain line, release wave in dashed line, black color : high pressure or tensile stress, gray color : low pressure or tensile stress) (b) experimental and caculated by HUGO and SHYLAC free surface velocity, with coating debonding. 1 : pull-back due to incident shock wave. 2' : pull back due to emergence of the part of the incident wave reflected at the fracture. 2'' : pull back due to the second emergence of this last wave. Substrate : Cu, coating : Elecrochemical Ni (125 um), Power densitty is 370 GW/cm^2. (From ref 3)

Figure 6 :SEM pictures of a rear surface of 50 µm thick aluminum target (τ = 300fs, Flux: 0.56PW/cm ^{2}.)

Figure 7 : Experiment-numerical comparison of a laser shot carried out in femtosecond regime. τ = 300fs, Flux: 0.56PW/cm ^{2}; 50µm thick aluminum target. Blue: experimental RSFV.Black : RSFV simulated without damage criteria and without 2TM. Green: RSFV simulated without damage criteria and with 2TM. Red: RSFV simulated with the Kanel criterion and with 2TM.

Figure 8 : Space-time diagram corresponding to the 23TW/cm^2 irradiation on multi-layer systems comprising a molybdenum metallic layer and a chalcopyrite $CuInSe_2$

semi-conductor film deposit on soda-lim glass substrate. Laser pulse duration is 300 fs. Simulation is performed using 1D SHYLAC code. Corresponding RFSV measurement and debonding threshold calculation is reported on diagramm. (From ref. 25)

Figure 9: Synopsis of the edge effect mechanisms involved into a short loading duration shock over a limited surface. Pressure evolution for various time steps after laser loading on a spot of 2mm diameter of an aluminum target. Calculation performed with 2D Radioss Code. (From Ref. 13)

Figure 10 : cross section micrography corresponding to experiments carried out on Al 2mm thick, a. Al 2mm thick, spot diameter: 4mm, pulse duration : 5ns, Power density :2.08 TW/cm^2 . b. spot diameter: 1mm, pulse duration : 5ns, Power density :1.88 TW/cm^2; (From Ref. 13)

Figure 11 : comparison of experimental free surface velocity signals and corresponding numerical simulation with Tuler-Butcher damage criterion for:Al 2mm thick, spot diameter: 1mm, τ=5ns, I=1.88 TW/cm^2 (From Ref. 13)

Figure 12 : Adhesion Test on TBCs : a.digital scan with modified contrast showing whitened spots on the top surface of TBCs after LASAT b.White spot diameter vs. Laser fluency plot for a LASATed TBCs. Laser spot laser is 2.5mm. (from ref. 5)

Figure 13 : Pressure distribution for a 1.25 mm diameter shock at 200 MPa peak stress.a. Incident shock wave, b. Reflected tensile wave and c. Max stress distribution along the interface (from ref. 5)

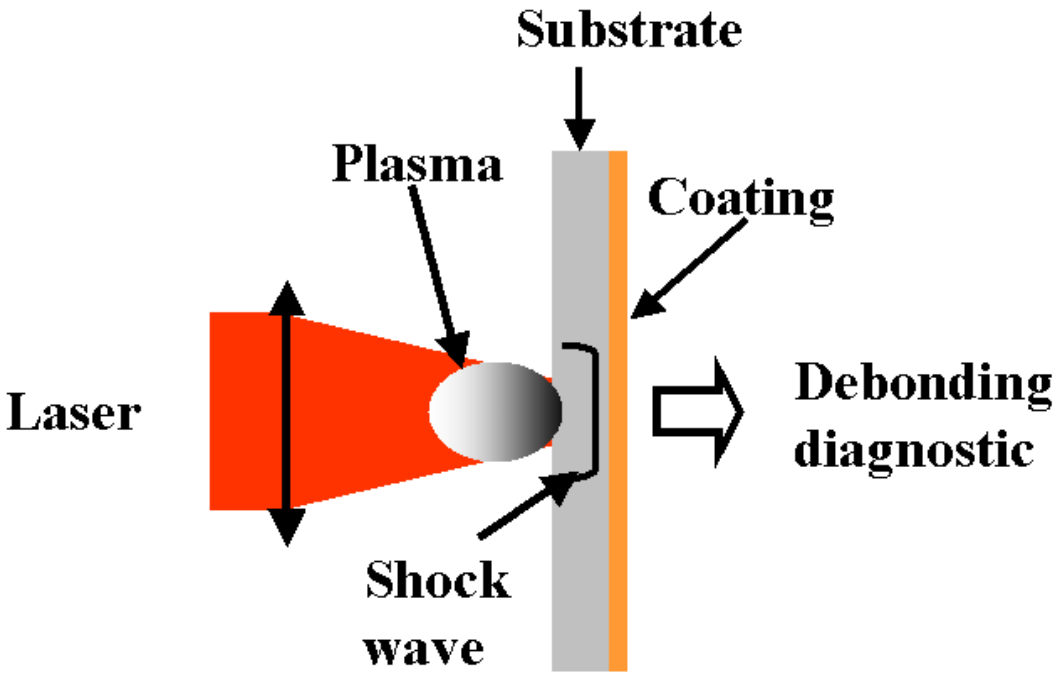
Substrate
Plasma
Coating
Laser
Debonding
diagnostic
Shock
wave

Figure 1

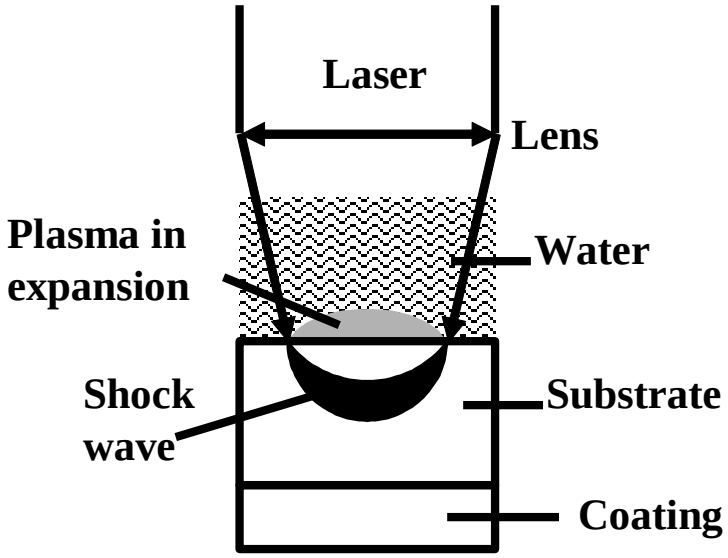
Laser
Lens
Plasma in
expansion
Water
Shock
wave
Substrate
Coating

Figure 2

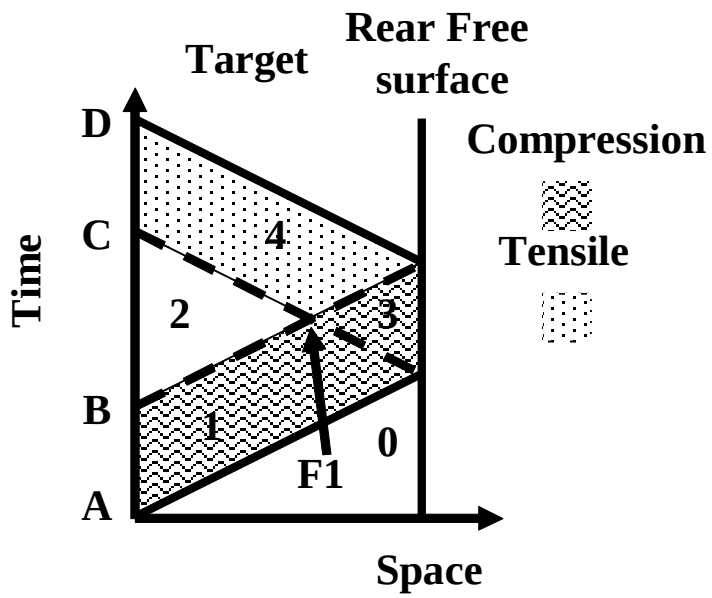
Target
Rear Free surface
Compression
Tensile
D
C
B
A
Time
Space
4
2
3
1
0
F1

Figure 3 a

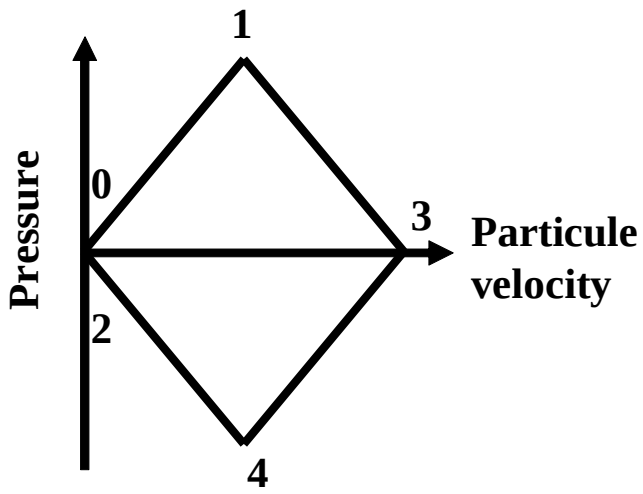

Figure 3 b

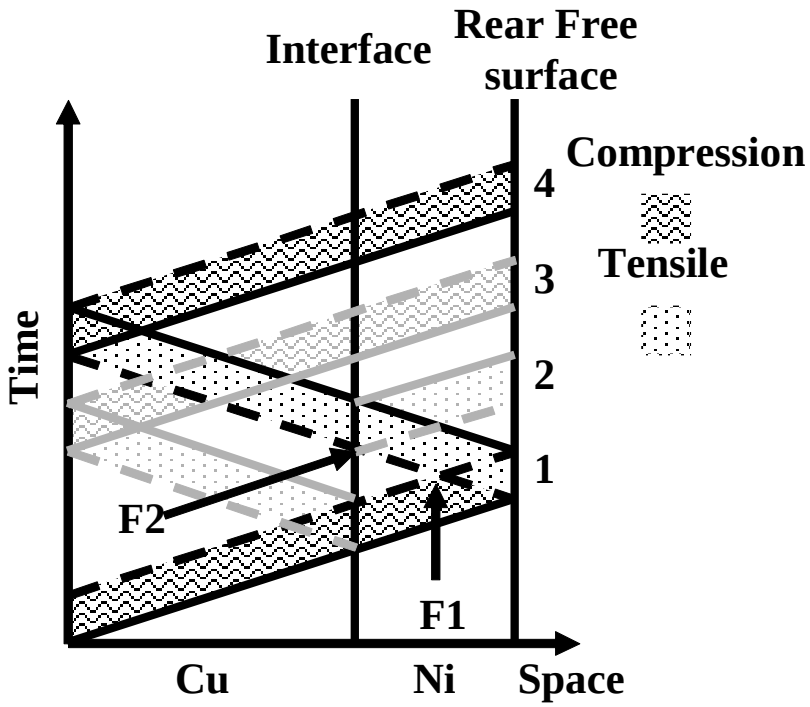
Interface
Rear Free surface
Compression
Tensile
4
3
2
1
Time
F2
F1
Cu
Ni
Space
Figure 4a

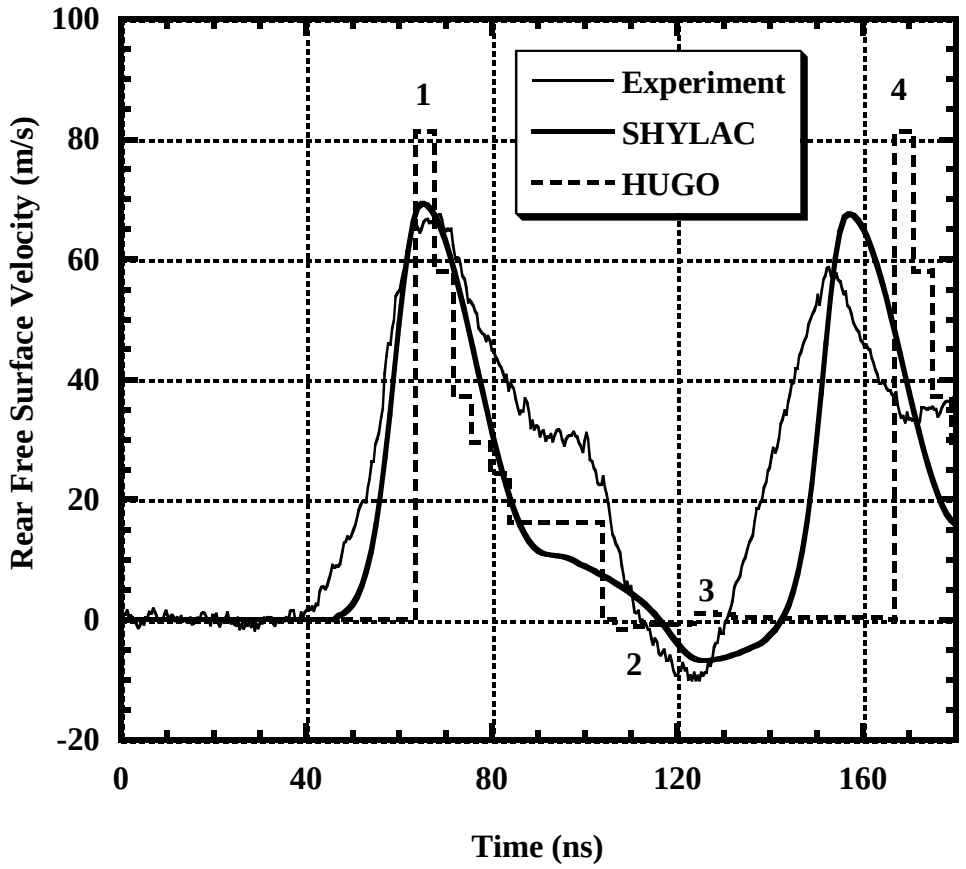
Rear Free Surface Velocity (m/s)
100
80
60
40
20
0
-20
0
40
80
120
160
Time (ns)
Experiment
SHYLAC
HUGO
1
2
3
4

Figure 4b

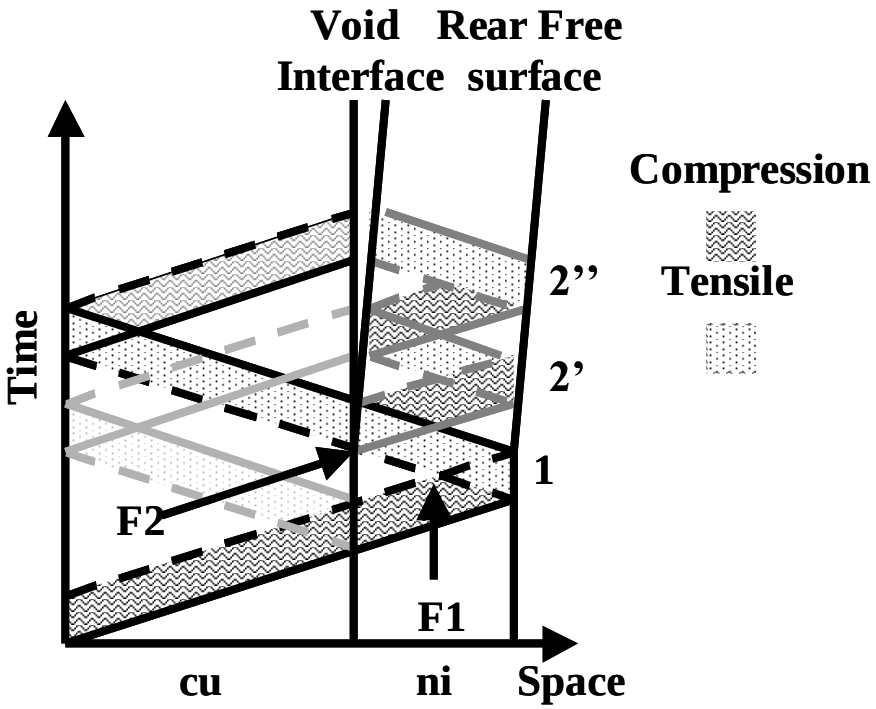
Void
Interface
Rear Free
surface
Compression
Tensile
Time
2''
2'
1
F2
F1
cu
ni
Space

Figure 5a

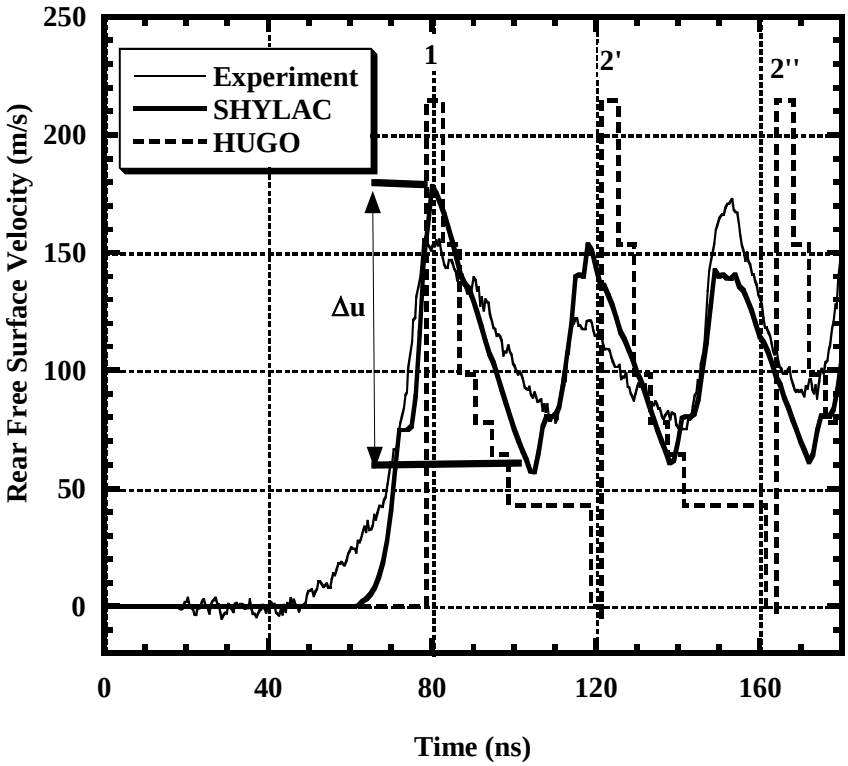
Experiment
SHYLAC
HUGO
1
2'
2''
Δu
Rear Free Surface Velocity (m/s)
Time (ns)
250
200
150
100
50
0
0
40
80
120
160

Figure 5b

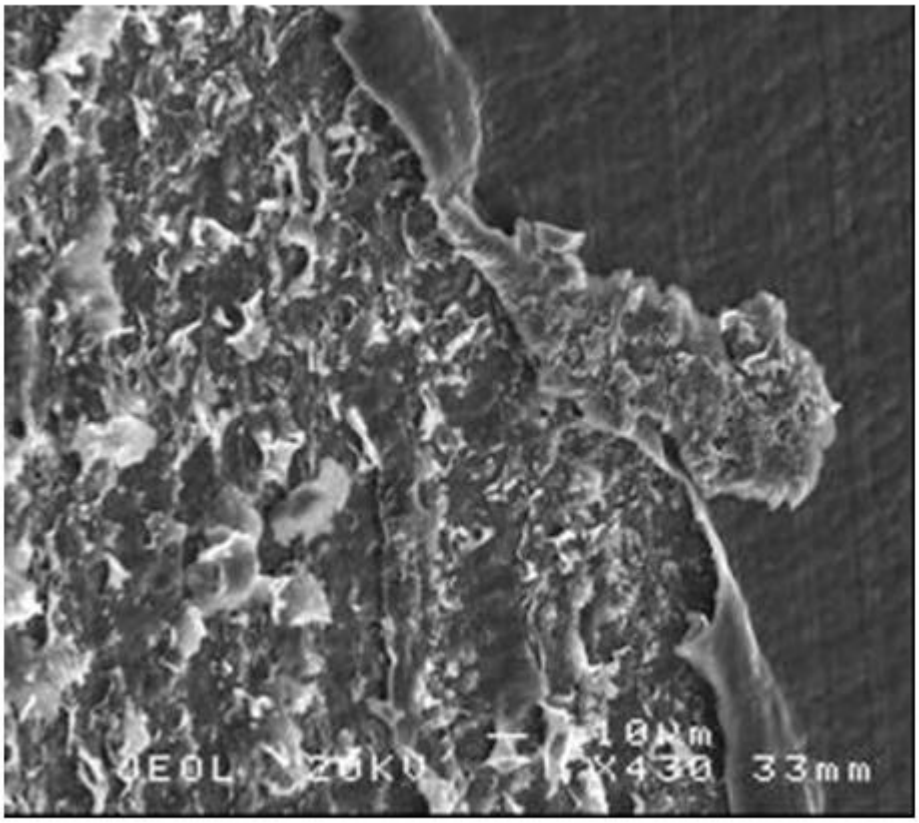

Figure 6

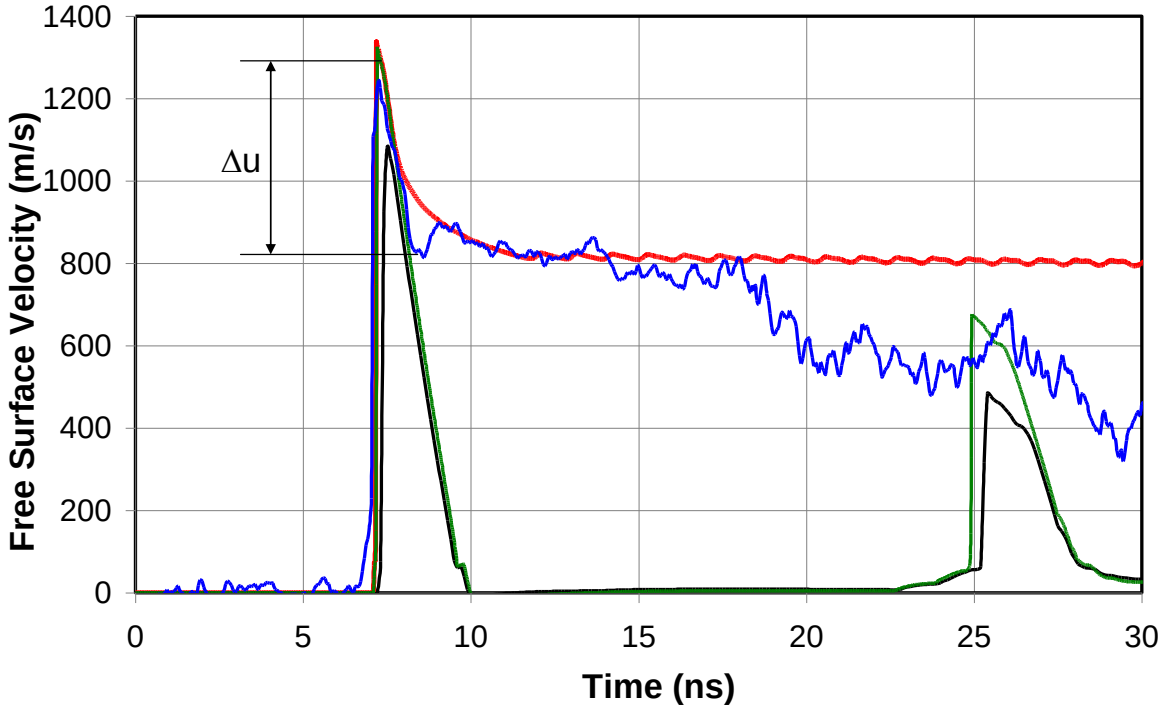
Free Surface Velocity (m/s)
1400
1200
1000
800
600
400
200
0
Δu
0
5
10
15
20
25
30
Time (ns)

Figure 7

Figure 8

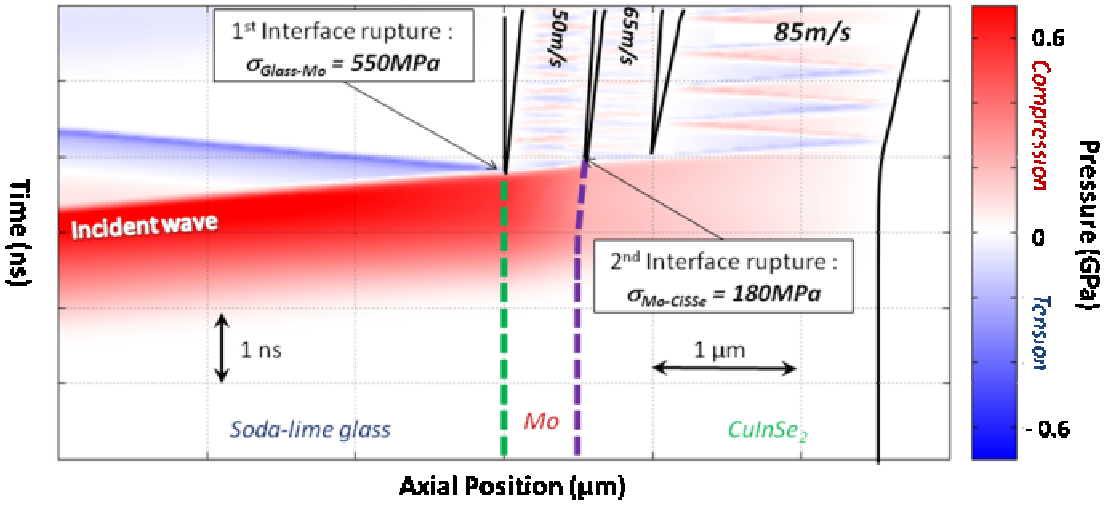

Figure 8

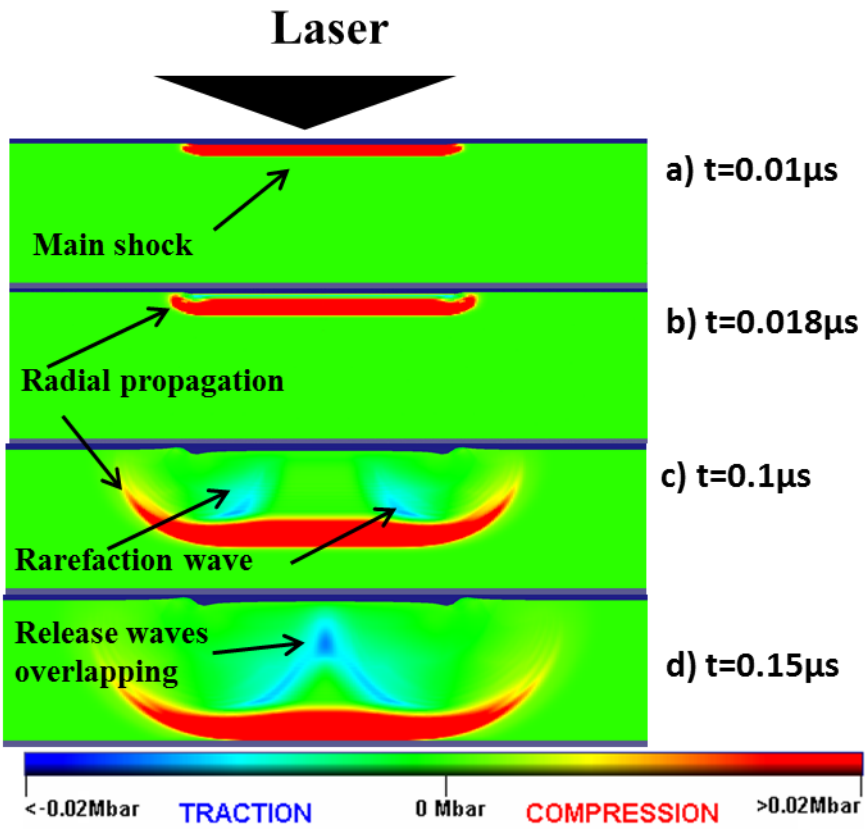
Laser
Main shock
a) t=0.01µs
Radial propagation
b) t=0.018µs
c) t=0.1µs
Rarefaction wave
Release waves
overlapping
d) t=0.15µs
<-0.02Mbar
TRACTION
0 Mbar
COMPRESSION
>0.02Mbar

Figure 9

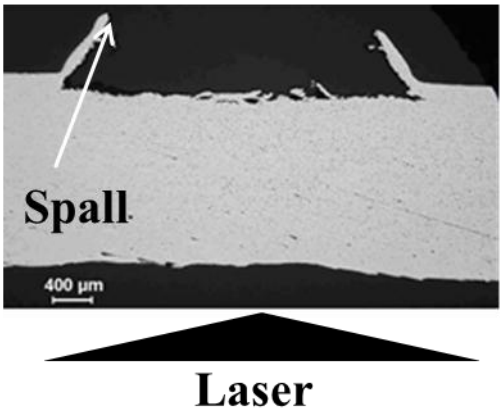

Laser

Figure 10a

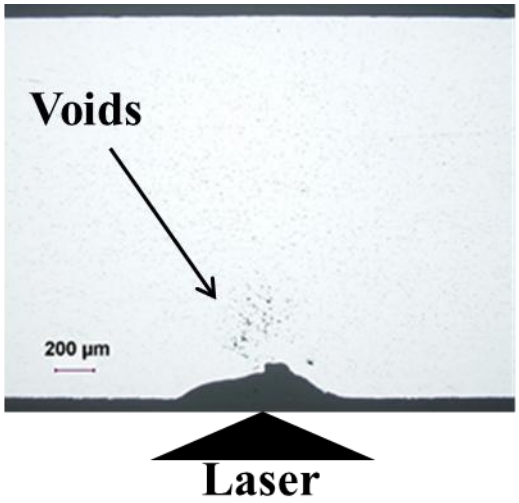

Figure 10**b**

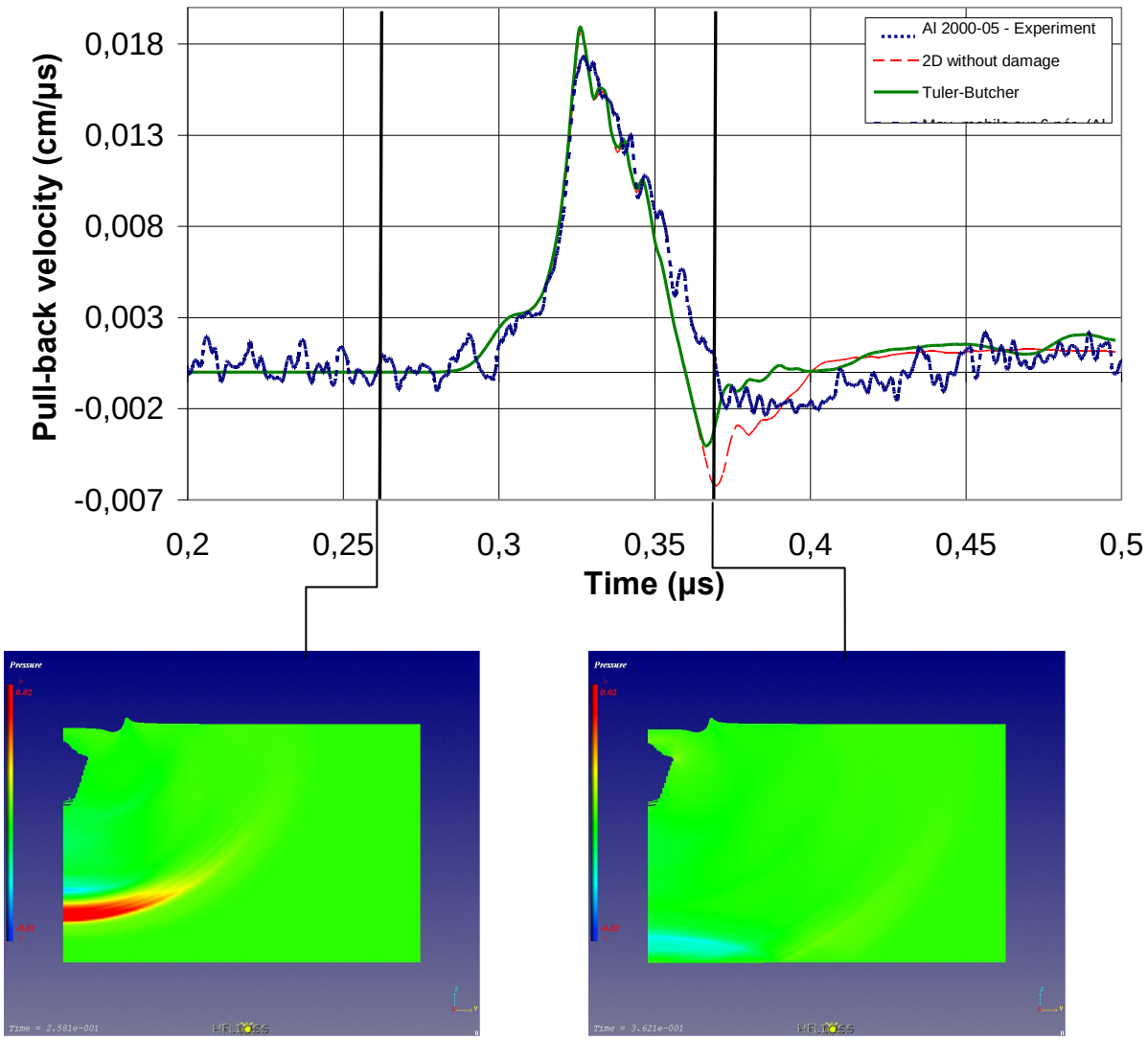
Al 2000-05 - Experiment
2D without damage
Tuler-Butcher
Pull-back velocity (cm/µs)
0,018
0,013
0,008
0,003
-0,002
-0,007
0,2
0,25
0,3
0,35
0,4
0,45
0,5
Time (µs)
Pressure
Pressure

Figure 11

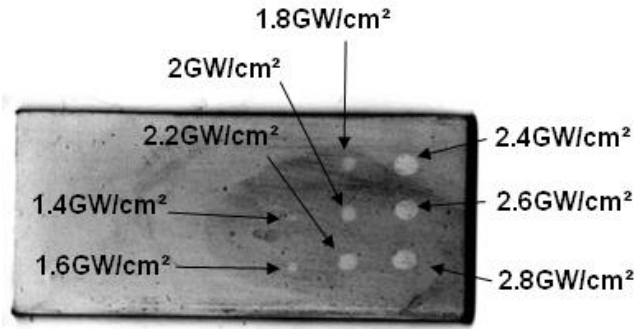
1.8GW/cm²
2GW/cm²
2.2GW/cm²
2.4GW/cm²
1.4GW/cm²
2.6GW/cm²
1.6GW/cm²
2.8GW/cm²

Figure 12**a**

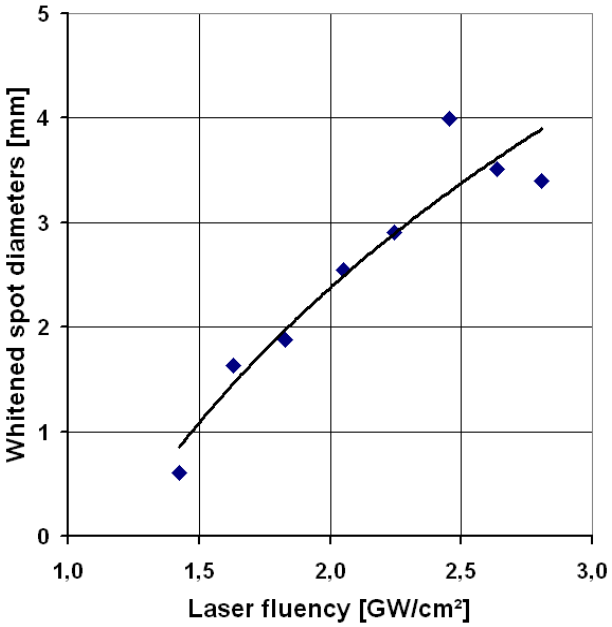
Whitened spot diameters [mm]
0
1
2
3
4
5
1,0
1,5
2,0
2,5
3,0
Laser fluency [GW/cm²]
Figure 12**b**

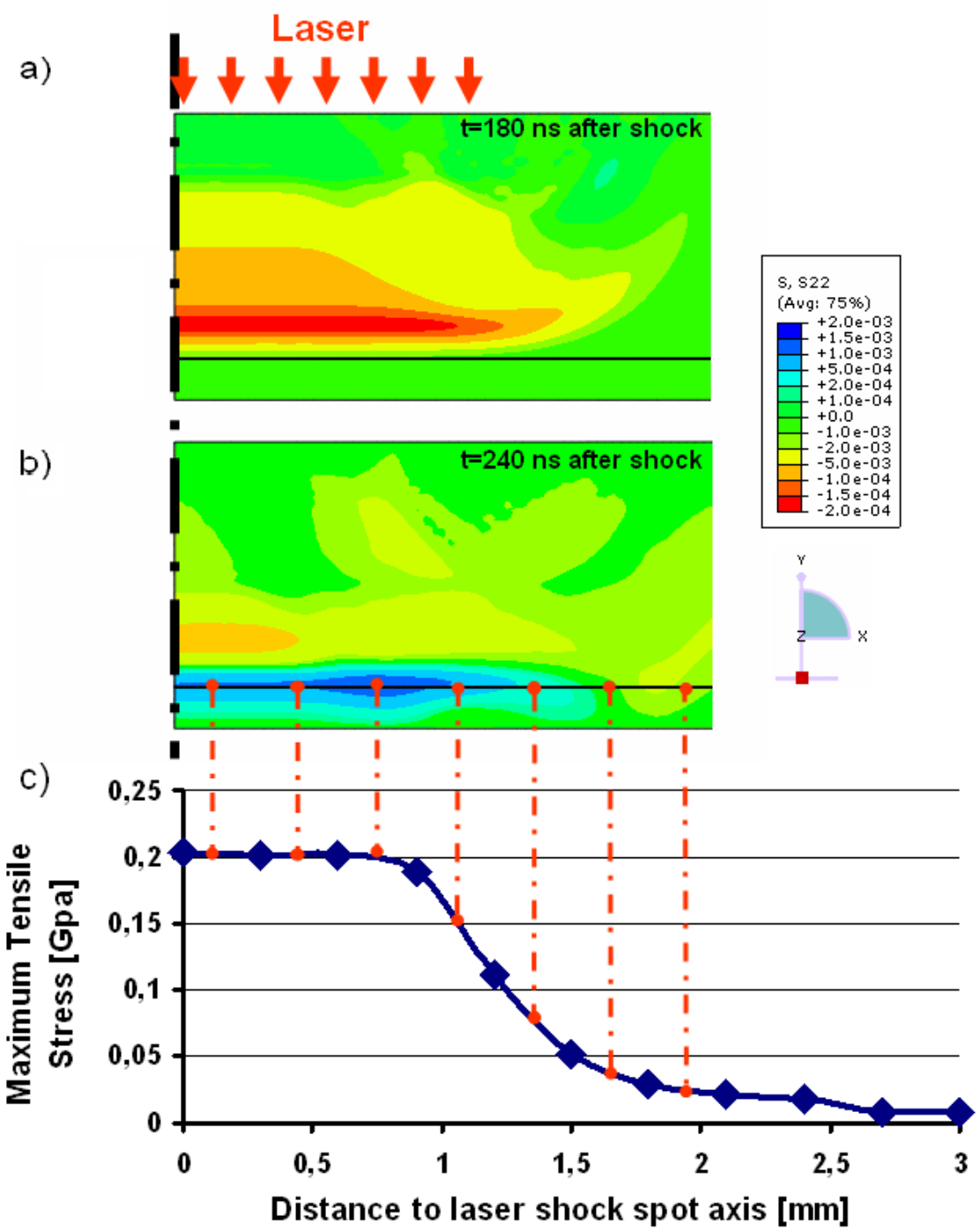

Figure 13